Combustion and Flame 188 (2018) 243–249

Contents lists available at ScienceDirect

Combustion and Flame

journal homepage: www.elsevier.com/locate/combustflame

Surface engineered nanoparticles dispersed in kerosene: The effect of oleophobicity on droplet combustion

Michael N. Bello[a], Kevin J. Hill[a], Michelle L. Pantoya[a,*], Richard Jason Jouet[b], Jillian M. Horn[b]

[a] Department of Mechanical Engineering, Texas Tech University, Lubbock, TX 79409, USA
[b] Indian Head Division, Naval Surface Warfare Center, Research and Technology Department, Indian Head, MD 20640, USA

ARTICLE INFO

Article history:
Received 24 March 2017
Revised 14 June 2017
Accepted 27 September 2017

Keywords:
Liquid propellants
Aluminum additives
Oleophobicity
Hydrophobicity
Boiling
Combustion

ABSTRACT

Liquid propellants benefit from solid particle additives that can optimize combustion performance by promoting phase change heat transfer. In this study, aluminum (Al) nanoparticles with and without self-assembled monolayer surface functionalization were combined with kerosene to examine the changes in droplet regression behavior associated with manipulating particle surface chemistry. Aluminum nanoparticles were coated using a long-chain perfluorinated carboxylic acid as the surface binding moiety to induce an oleophobic surface. The resulting particles are thus comprised of self-assembled monolayers of perfluorohexadecanoic acid (PFHD) ($C_{15}F_{31}COOH$) around the alumina (Al_2O_3) shell encapsulating the Al core. The PFHD serves many functions including altering particle wettability and acting as a surfactant that facilitates a stabilized dispersion of particles in kerosene. The Al-PFHD particles are more oleophobic compared with the more oleophilic surface associated with the amorphous alumina shell on aluminum particles. Mixtures with Al-PFHD exhibit a two stage burning behavior with average initial burn rate constant increased by about 121% when compared to pure kerosene. Further analysis using a thermogravimetric analyzer (TGA) showed that Al-PFHD particles in kerosene exhibit evaporation at reduced temperatures that may enhance energy transport during droplet combustion by phase change and convection. These results provide new insight bridging the gap between materials and heat transfer toward achieving the goal of designing particle additives that improve liquid propellant combustion.

1. Introduction

Regression rate is an indicator of liquid propellant combustion performance and defines the rate that a droplet surface recedes over the course of its combustion [1]. Higher regression rates indicate faster combustion of the liquid fuel, which is usually desirable. An approach for improving the regression rate of liquid propellants is to include particulate additives that affect burning behavior by promoting heat transfer that leads to faster regression rates and improved combustion. Understanding the mechanisms for how particulate additives affect combustion is important for optimizing performance of next generation liquid fuels.

There are three basic approaches for selecting particulate additives to liquid propellants: (1) exploit chemical energy associated with metal fuel particles (such as aluminum [2–4]) toward providing more chemical energy within the mixture that can be liberated upon reaction; (2) identify materials that may spur catalytic exothermic reactions with the propellant (such as iron oxide, Fe_2O_3, or cerium(IV) oxide, CeO [5]) and may increase the rate chemical energy is liberated upon reaction; and (3) optimize the number of nucleation sites within the liquid to activate phase change heat transfer at lower temperatures and promote improved combustion [4]. The first two approaches are basically driven by chemical mechanisms to enhance either overall energy liberated or the rate that energy can be liberated during droplet combustion. The third approach relies more heavily on accelerating combustion through heat transfer driven by nucleation sites within the multiphase mixture. Phase change can enhance heat transfer because latent heat is typically much larger than sensible heat. For example, the latent heat needed to boil 1 gram of kerosene ($h = 251$ J/g) is about 25 times larger than the heat required to increase the temperature of the same amount of kerosene by 5 K (10 J/g). In addition, phase change is frequently accompanied by fast and large changes in specific volume that results in enhanced heat transfer due to convection. These processes will significantly contribute to enhancing droplet combustion.

* Corresponding author.
E-mail address: michelle.pantoya@ttu.edu (M.L. Pantoya).

https://doi.org/10.1016/j.combustflame.2017.09.041
0010-2180/

While the approach taken in this study uses aluminum (Al) particles, the mechanisms associated with activating phase change heat transfer is the focus of this study. The hypothesis is that high heat transfer rates associated with surfaces that promote phase change and nucleate boiling will improve combustion more than simply the addition of nanoparticle aluminum (i.e., nano Al) additives. Toward this end, two different particle additives were examined: aluminum particles compared with the same aluminum particles with a surface functionalization to alter the wettability of the particle.

The quasi-steady process of nucleate boiling involves the temporal sequence of nucleation, bubble growth and detachment. Heat is exchanged optimally when the solid particle surface is in contact with both the vapor and liquid phase [6]. Therefore, a strategy for designing optimum particle surfaces relies on controlling the surface structure to promote contact with both the continuous (liquid) and discrete (vapor) fluid phases. One way to achieve a prescribed surface architecture is by processing techniques that alter surface chemistry; such as by depositing low-surface energy materials (e.g., fluoropolymers) that will induce surface hydrophobicity (i.e., water repelling) and oleophobicity (i.e., oil repelling) properties, and promote multiphase interfaces. In this case, the substrate is amorphous alumina, the passivation shell on aluminum particles. A perfluoro-organic acid was chosen as the coating species to induce greater oleophobicity that will affect nucleate boiling of kerosene and improve droplet combustion [7]. This approach could also be extended to manipulate particle hydrophobicity to impact more polar liquid fuels.

The purpose of this study is to exploit the surface chemistry associated with a perfluorinated self-assembled monolayer (SAM) coating on Al nanoparticles toward optimizing nucleate boiling and improving droplet combustion. This is accomplished by experimentally measuring droplet surface burn rates for kerosene combined with 0.5 wt.% nano Al particles, and kerosene combined with the same concentration of nano Al particles functionalized with perfluorohexadecanoic acid (PFHD) SAMs. Further characterization diagnostics include thermal gravimetric analysis (TGA) for evaluation of phase change behaviors; as well as Fourier transform infrared spectroscopy (FTIR) for evaluation of surface features of Al-PFHD particles; and Laser Flash Analysis (LFA) to quantify the differences in thermal properties of the sample mixtures. Results shown here extend the usefulness of surface engineered materials to applications involving liquid propellants, a medium not previously studied using particles with SAM coatings to control surface wettability as a parameter affecting combustion.

2. Experimental

2.1. Materials

The base propellant used for this study is kerosene ($C_{12}H_{26}$), from Sigma Aldrich (St. Louis, MO). Kerosene is refined from petroleum oil and a commonly used surrogate for aviation fuel [8]. Kerosene is non-polar and has oil-like properties as opposed to water-like properties. Therefore, particle surface engineering must be designed to produce oleophobic rather than hydrophobic properties. This is most commonly achieved with fluorocarbon coating materials.

The aluminum (Al) particles have an 80 nm average diameter and were procured from Nova Centrix (Austin, TX). The Al particles are passivated with an alumina (Al_2O_3) shell with an average thickness of 3 nm, and were well characterized by Kappagantula et al. [9]. In addition to this baseline Al powder, the same Al powder was also functionalized with self-assembled monolayers (SAM) prepared from a perfluorinated carboxylic acid, specifically, perfluorohexadecanoic acid (PFHD). The procedure for accomplishing similar functionalization is well described in [10] and [11] to obtain particles hence forth referred to as Al-PFHD, with 35 wt.% acid concentration consuming an average corona thickness of 5 nm (similar to [9]). The powder product was washed three times in diethyl ether to remove any acid that was not bonded to the alumina shell. The dried powder was reclaimed for further experimentation as described below.

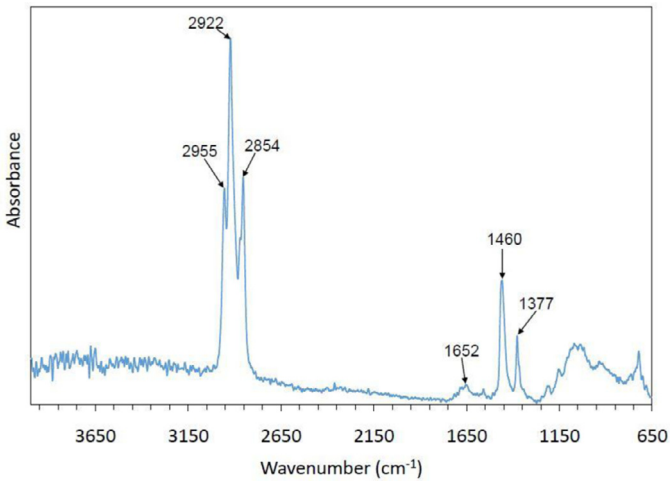

Fig. 1. Spectrum of Al-PFHD in kerosene using ATR-FTIR.

The Al-PFHD powder was examined using Fourier transform infrared spectroscopy (FTIR) with a Tensor 27 manufactured by Bruker Optics (Billerica, MA). Samples of roughly 10 mg quantity were loaded on an attenuated total reflectance (ATR) accessory and scans were made at a resolution of 1 cm^{-1}. The analysis was performed to characterize PFHD bonding to the Al particle surface, which is an extension to previous FTIR analysis of perfluorotetradecanoic acid (PFTD) coated Al particles [10].

Figure 1 shows peaks in the 1300–1500 cm^{-1} region associated with C–F stretching modes and the 2800–3000 cm^{-1} region is associated with O–H stretching modes [10]. The presence of C–F groups suggests $C_{15}F_{31}COOH$ remains intact upon absorption to the alumina surface. Another observation is an absence of the carbonyl stretching mode at 1754 cm^{-1} but there are multiple O–H stretching modes 2854–2954 cm^{-1} such that the carboxylic acid may absorb to the alumina surface through scission of O–H bonds and consequently results in the formation of a carboxylate species. This was observed previously for PFTD on Al [10] such that the bonding behavior for Al and PFTD appears similar to Al and PFHD.

The mixtures were analyzed for their bulk thermal properties using a Netzsch Laser Flash Analyzer (LFA) 447 at 25 and 50 °C for each sample. Approximately 0.3 cm^3 of kerosene, Al with kerosene, and Al-PFHD with kerosene were prepared and analyzed. Multiple tests with thirty measurements per test were evaluated and averaged to ensure repeatability of the measurement. This analysis was performed to understand how the bulk thermal properties of the mixtures vary as a function of particle composition. Table 1 includes the measured average thermal diffusivity for each sample at 25 and 50 °C. The variation in measured thermal diffusivity is relatively constant among all samples and consistent with reported literature for kerosene [14].

2.2. Burn rate constant measurements

Droplet burning behavior was experimentally observed using a modified apparatus as explained Datta et al. [12] and Bello et al. [13]. A 50 μm diameter quartz fiber with a circular cross-section acted as the support for fuel droplet suspension. It is also noted

Table 1
Measured thermal diffusivity and standard deviation of five measurements for each sample at 25 and 50 °C.

Sample	Thermal diffusivity (mm^2/s) @ 25 °C	Thermal diffusivity (mm^2/s) @ 50 °C	Standard deviation @ 25 °C	Standard deviation @ 50 °C
kerosene	0.073	0.072	0.003	0.002
Al + kerosene	0.074	0.075	0.005	0.003
Al-PFHD + kerosene	0.073	0.073	0.003	0.002

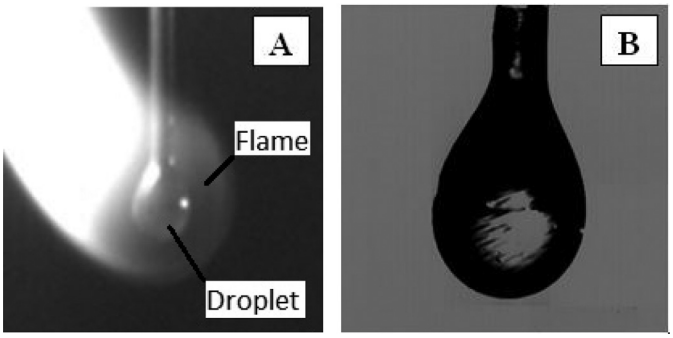

Fig. 2. High speed images of (A) actual burning droplet and (B) burning droplet viewed in Vision Research software.

that the same fibers were used for all samples investigated to ensure consistency such that the trends in behavior among dispersions are repeatable.

Droplets were introduced onto the quartz fiber using a syringe. The shape of the suspended droplet on the support fiber was naturally distorted from spherical to ellipsoidal owing to gravity effects. To minimize the settling of the particles resulting from gravity, the mixtures were used less than an hour after sonication. The maximum diameter was measured as a function of time. All experiments were performed in triplicate to establish repeatability.

A bent wire attached to an acrylic plate is positioned underneath the droplet and connected to a voltage source to resistively heat the wire and ignite the fuel droplets. A consistent 3-V AC current was supplied to the wire and all samples achieved ignition. The droplet is enclosed in a combustion chamber of quiescent ambient air at standard temperature and pressure to reduce air circulation around the droplets. A Phantom IV (Vision Research, Wayne, NJ) high-speed camera was used to image droplet regression rates. A K2 Long-Distance Microscope lens (Infinity Photo-Optical Company, Boulder, CO) was attached to the high-speed camera for higher magnification. A fiber optic light source (Cole Parmer® Illuminator, 41720 series) was used to increase the contrast between the droplets and background for improved visualization. Figure 2A and B shows high speed images of a burning droplet and a burning droplet as seen in the Vision Research software. The edges of the droplet are traced (in pixels) throughout the burning process and converted to diameter. These diameters measured alongside time scales were used to determine burn rate constants.

All data processing was performed off-line using a commercial software package MATLAB R2015aSP1 (The MathWorks Inc., Natick, MA). The code was programmed and used to examine the burn rate constants (obtained from transient diameter squared data) for each test. The code calculated the percent difference of the linear trend line R^2 value of the two changing segments for each data set. When the percent difference in R^2 values rose above 1%, indicating increased linearity in at least one of the changing segments compared to the full data set, the code output the slope and R^2 value of each stage. This allowed quantitative evaluation of the two-stage burning behavior.

2.3. Thermal equilibrium analysis

Thermal analysis was performed using a Netzsch STA 449 differential scanning calorimeter (DSC) and thermogravimetric analyzer (TGA). Samples were prepared by sonication of Al or Al-PFHD in kerosene. The 20 mg samples, kerosene, Al with kerosene, and Al-PFHD with kerosene, were loaded into the DSC/TGA and heated to 800 °C at 10 °C/min in an argon environment.

3. Results

As mentioned in the introduction, tailoring surface chemistry is an approach to altering surface properties while maintaining bulk properties of a material. In the case of Al-PFHD, the PFHD SAM is approximately 5 nm thick and does not significantly alter the thermal transport properties of the mixture (Table 1). This data confirms that while PFHD may be more insulative than the conductive metal particle, the composite and low particle concentration in the kerosene (i.e., 0.5 wt.%) does not affect the mixture's thermal diffusivity, even at slightly elevated temperatures.

The aluminum particle surface is amorphous alumina, and when functionalized with PFHD, the surface properties change. In particular, applying a fluoropolymer coating to alumina surface alters the wettability of the surface. Wettability describes the spreading of a liquid on a surface and is characterized by contact angle at the solid–liquid interface. A surface is wetting when a liquid that forms a contact angle with the solid surface is less than 90° and the solid surface is referred to as oleophilic or hydrophilic depending the oil or water properties of the liquid, respectively. Alumina is naturally oleophilic and hydrophilic [15]. Contact angles associated with the particle surfaces used here are difficult to measure owing to the nano-scale curvature of the particles. Compressing powder into consolidated pellets and applying a droplet to the pellet surface using goniometry to measure contact angle is one approach for representing the hydrophobic or oleophobic properties of the surface. However, in this study, powders that were compacted resulted in droplets permeating the powder before accurate contact angle measurements could be made.

Fluoropolymer surfaces are naturally more hydrophobic and oleophobic than alumina. Research on fluorocarbon SAMs with polar and non-polar liquids has shown that the degree of hydrophobicity and oleophobicity is a function of the chain length of the fluorocarbon [16,17]. As the SAM chain length increases up to about six carbon atoms, the contact angle also increases for a SAM coated surface and similar hydrocarbon fuels to kerosene. For fluorinated carbon chain lengths beyond 6, the contact angle plateaus to a constant value of about 90° for similar hydrocarbon fuels. In the case of PFHD, a 15 carbon length chain, contact angles approaching 90° are anticipated. Even without a representative measurement for the Al-PFHD surfaces, the data from [16,17] suggest the Al-PFHD surface is more oleophobic and more hydrophobic compared to the Al particles without a fluorocarbon SAM. Another observation of this difference is seen in the dispersion behavior of the particles in kerosene. Figure 3 shows vials of kerosene with Al, and kerosene with Al-PFHD with the more oleophobic Al-PFHD particles clearly suspended for up to 2 days while the Al particles settle within 2 h.

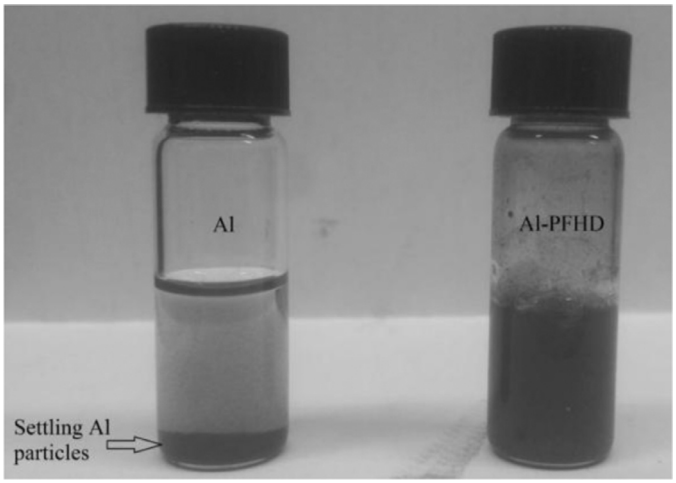

Fig. 3. Suspension of Al and Al-PFHD in kerosene after 2 h. Note: Al in kerosene settles at the bottom of the vial whereas Al-PFHD is still well dispersed throughout the liquid.

When kerosene is combined with oleophobic compared with oleophilic powders at the same concentration, combustion behaviors are appreciably different. Figure 4 shows normalized droplet diameter squared as a function of time for the three samples investigated. Droplet diameter squared, D^2, is normalized against the initial droplet diameter, $D_o{}^2$. The burn rate constant, K_b is calculated as the slope of the diameter squared versus time plot ($K_b = d(D^2)/dt$) [18]. All samples show a two stage linear burning behavior (i.e., Stages 1 and 2), distinguished by linear trend lines fit to the slopes of each stage shown in Fig. 4. The stages are delineated by the first point that the linearity of the second stage increases by 1% or more compared to the linearity of the full data set. Stage 1 is more generally an initial heating period for pure kerosene but associated with combustion for both particle laden droplets; and Stage 2 is more aggressive combustion of the kerosene droplet marked by a steeper slope and nearly the same rate for the particle laden droplets, suggesting steady combustion that is no longer influenced by the surface properties of the particles.

Table 2 shows burn rate constants K_b for each sample and each stage of combustion, respectively. It is noted that based on repeatability, the largest source of uncertainty in the regression rate measurement is 0.5%.

Figure 5A and B shows mass loss with TG and DTG plots of three samples (i.e., pure kerosene, Al with kerosene, and Al-PFHD with kerosene) as a function of temperature at a heating rate of 10 °C/min, respectively. Figure 5A shows there is a mass loss starting at 85 °C for the Al-PFHD in kerosene, with derivative thermo-

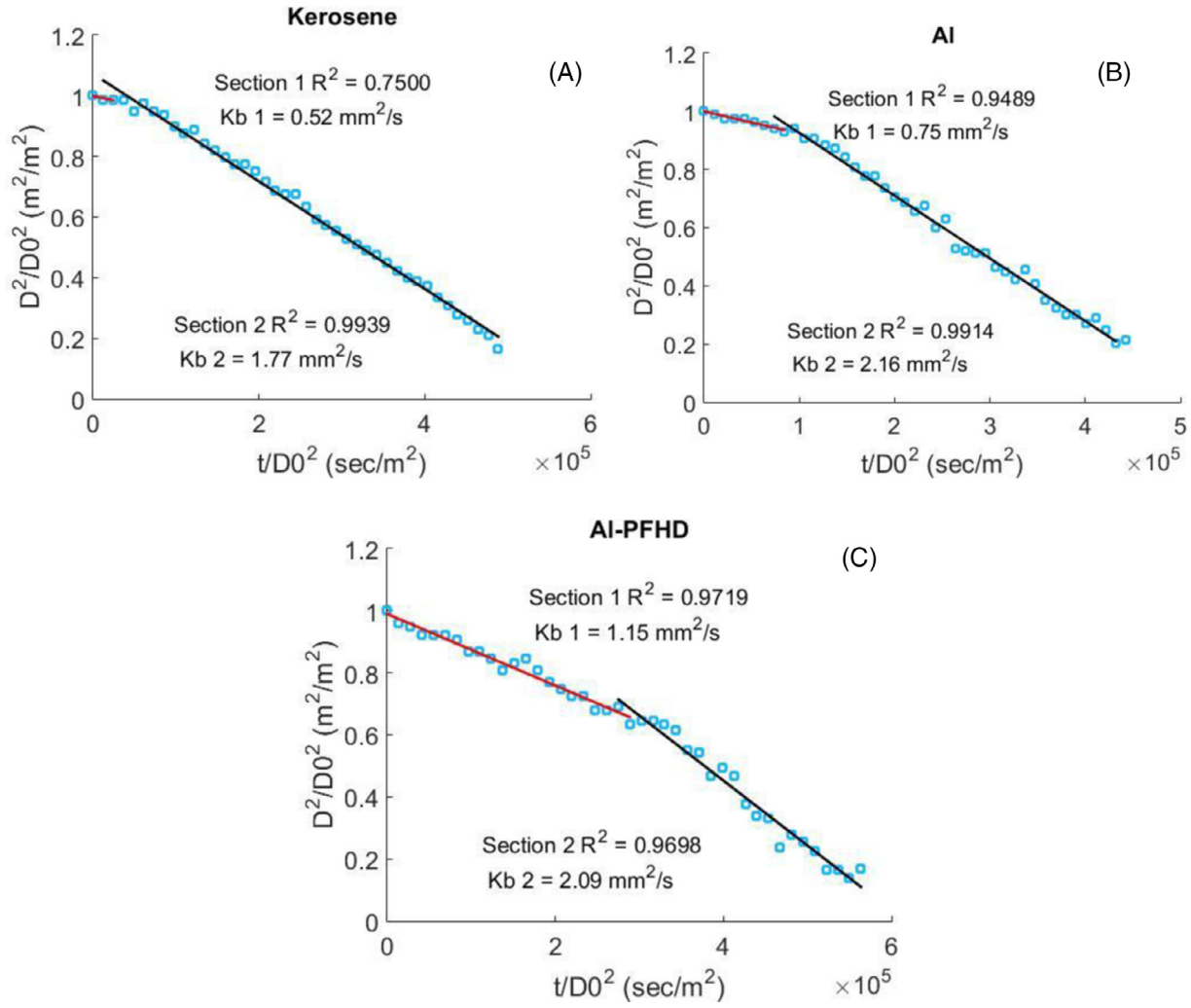

Fig. 4. Droplet diameter squared histories for: (A) kerosene; (B) kerosene with 0.5 wt.% Al; and (C) kerosene with 0.5 wt.% Al-PFHD. Note: the linear trend line slopes representing distinct stages in burning behavior as noted by the burn rate constants (K_b) for Stages 1 and 2, respectively.

Table 2
Results for kerosene showing total combustion time duration (in seconds) and burn rate constants for stages of regression with 0.5 wt.% Al and Al-PFHD.

Additive in kerosene	Burn time (s)	Stage 1 K_b (mm²/s)	Stage 2 K_b (mm²/s)
None	2.90	0.52	1.77
Al	2.45	0.75	2.16
Al-PFHD	2.05	1.15	2.09

Table 3
Data for mass loss, onset temperatures, and mass loss percentages of mixtures in Fig. 5A. Note: N/A indicates not applicable because the kerosene and kerosene with Al mixture do not exhibit early stage mass loss.

Sample	Stage A mass loss onset temp (°C)	Stage A mass loss (%)	Stage B mass loss onset temp (°C)	Stage B mass loss (%)	Overall mass loss (%)
Kerosene	N/A	N/A	135	95.70	95.70
Al + kerosene	N/A	N/A	105	97.16	97.16
Al-PFHD + kerosene	85	7.25	123	90.70	97.95

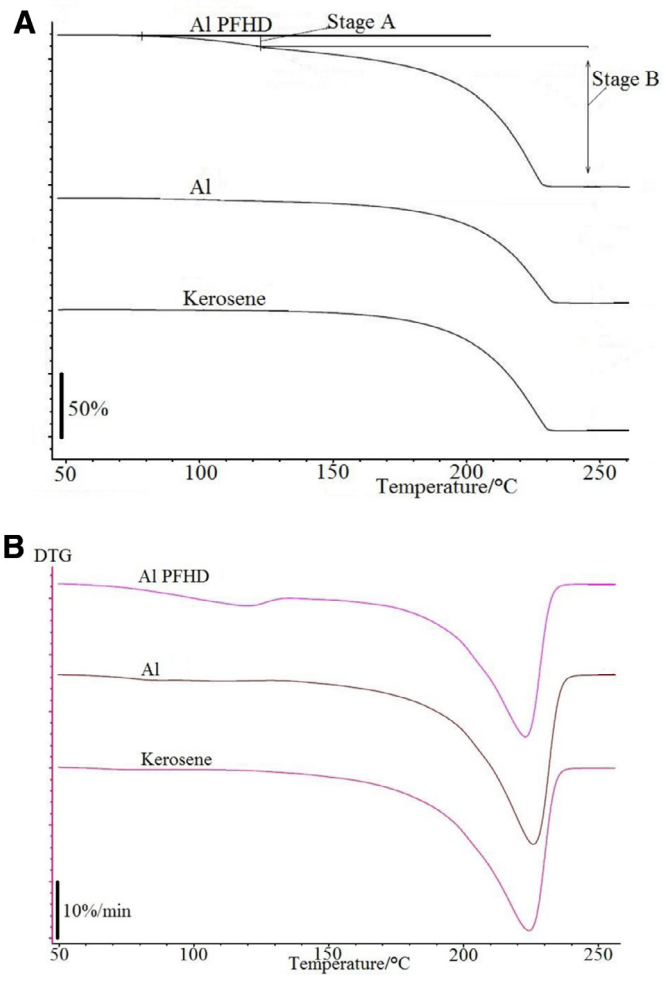

Fig. 5. (A) TG mass loss curves for kerosene (bottom plot), Al with kerosene (middle plot), and Al-PFHD with kerosene (top plot) as a function of temperature for a constant 10 °C/min heating rate in an argon environment. Note: the two stage mass loss behavior associated with the Al-PFHD + kerosene sample identified as Stages A and B. (B) DTG of kerosene (bottom plot), Al with kerosene (middle plot), and Al-PFHD with kerosene (top plot) as a function of temperature for a constant 10 °C/min heating rate in an argon environment.

gravimetric (DTG) mass loss also shown in Fig. 5B. All mixtures evaporate prior to reacting under equilibrium conditions. From Fig. 5A, a mass loss of about 96–98 wt.% is shown for every sample; but the Al-PFHD exhibits a two stage mass loss as indicated in Table 3 and Fig. 5B.

4. Discussion

The contribution of Al-PFHD to burning behavior is shown in Fig. 4 by higher burn rate constants in the initial stage of combustion. In fact, compared to pure kerosene, droplets with Al-PFHD exhibit 121% increase in burn rate constant and droplets with Al exhibit a 44% increase in burn rate constant when compared to pure kerosene (Table 2). From visual observation the short duration of Stage 1 for pure kerosene (Fig. 4A) is associated with a heat up period while the longer duration of Stage 2 is kerosene combustion with a burn rate constant of 1.77 and an overall burn time of 2.90 s (Table 2).

The initial heating period seen for kerosene is replaced with combustion when particles are introduced into the droplet. The oleophobic particles (i.e., Al-PFHD) exhibit more aggressive burning behavior in Stage 1 with a higher burn constant than the Al particles (i.e., 1.15 compared with 0.75, see Table 2). Combustion for liquid hydrocarbons, like kerosene, occurs in the gas phase, such that that liquid–gas phase transition is a precursor to combustion [18]. Inciting this phase change at lower temperatures and/or earlier times should improve combustion as observed through higher burn rate constants at early stages. For the particle laden droplets, after this initial stage, the burn rate constant in Stage 2 for both samples is about the same, indicating steady state burning behavior is no longer a function of the surface properties of the particles. This observation suggests that the driving mechanism for reducing burn time is promoting phase change during early stages of combustion, this can be accomplished by manipulating the surface properties of the particles to promote evaporation and therefore combustion.

Data from TG and DTG analysis presented in Fig. 5 and Table 3 show that for Al-PFHD with kerosene, a two-stage evaporation process appears with the first stage beginning at 85 °C. Kerosene boils at 176 °C while PFHD melts at 115 °C and boils at 211 °C [19]. At 85 °C, the PFHD should remain in the solid phase. Figure 5A shows that for pure kerosene, evaporation begins at an onset temperature for mass loss of 135 °C (less than the reported bulk temperature of 176 °C). Reducing the phase change onset temperature to 85 °C shows that the oleophobic Al-PFHD particles reduce the onset of evaporation by 50 °C. Oleophilic surfaces, such as the Al particle surfaces, also promote nucleate boiling, albeit less efficiently as observed in Table 3 with lower burn rate constant. The onset temperature for phase change of the Al particles is reduced from 135 °C (for pure kerosene) to 105 °C, a reduction of 30 °C. While this data was collected under equilibrium conditions, the results suggest that the oleophobic Al-PFHD surface induces phase change at lower temperatures which may contribute to the higher burn rate constants for Stage 1 observed in

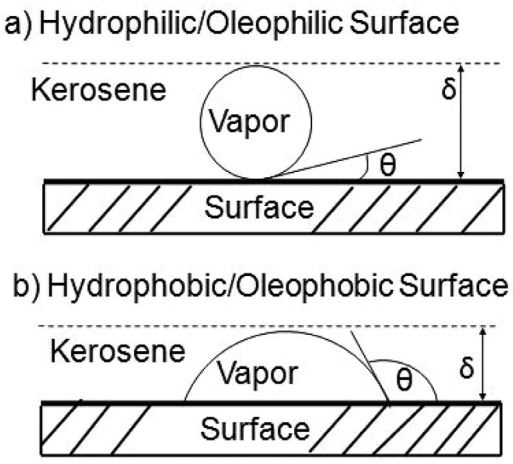

Fig. 6. Schematic of a kerosene droplet on an (a) oleophilic surface and (b) oleophobic surface. The dashed line parallel to the solid surface indicates the top of the limiting thermal boundary layer. The width of this layer is labeled δ. The contact angles (θ) define the smallest angle made between the liquid–vapor and liquid–solid (particle) interfaces.

Fig. 4C. The Al particles also induce phase change at lower temperatures than pure kerosene (Fig. 5B), but less dramatically than Al-PFHD owing to the Al particle surface that is more oleophilic. The reduction in phase change onset temperature associated with Al particles is also reflected in burn rate constant of Stage 1 compared with pure kerosene, in Fig. 4A and B. After Stage 1, the burn rate constants for the particle laden droplets are about the same while the pure kerosene droplet is slower; indicating the presence of particles overall enhances burn rate constant for the liquid fuel.

Figure 6 is a schematic of vapor bubbles and liquid kerosene in contact with an oleophilic and oleophobic particle surface. As the temperature of the particles rise faster than the liquid (owing to thermal properties differences), particle surfaces act as heaters to the surrounding liquid. The contact angles, θ, shown in Fig. 6 are the smallest angles made between the liquid–vapor and liquid–solid interfaces of the respective systems. Kerosene easily wets an oleophilic surface resulting in small contact angles whereas oleophobic surfaces are not easily wet and exhibit large contact angles. The limiting thermal boundary layer, δ, is shown as a dashed line parallel to the respective particle surfaces in Fig. 6. The thermal boundary layer is defined here as the layer of kerosene adjacent to the particle surface that is hot enough to support the growth of the vapor-phase bubble and extends a distance from the surface at which the temperature is 99% of the bulk liquid temperature. In a transient heating process, δ is not constant but grows in time. Faster heating rates (such as with the oleophobic particles) will result in smaller δ and conversely, slower heating rates (such as with the oleophilic particles) will result in larger δ. In Fig. 6, the wetting behavior of the surface plays a significant role in the growth of bubbles limited in size by δ. For a given δ, bubbles formed on oleophobic surfaces will have larger solid–vapor interfacial areas than those formed on oleophilic surfaces. Because heat transfer is lower through vapor than liquid, bubble growth at oleophobic surfaces is expected to be accompanied by a greater increase in temperature difference and heat flux than bubble growth at oleophilic surfaces. This mechanism may explain the results in Figs. 4 and 5 showing faster burn rate constants in oleophobic compared with oleophilic surfaces (Fig. 4); and, reduced onset of liquid–vapor phase change for oleophobic compared with oleophilic surfaces (Fig. 5).

The simple model in Fig. 6 accounts for the effect of surface wetting properties on the growth of bubbles already formed and whose uppermost interface is in contact with the limiting thermal boundary layer. It is consistent with the difference, after nucleation occurs, observed in regression rate for oleophobic and oleophilic surfaces. However, in order to interpret the onset temperatures observed in Fig. 5A for phase change, it is important to consider bubble formation as well as bubble growth.

Bubble nucleation at a surface immersed in a liquid can occur at a solid surface (heterogeneous nucleation) or within the bulk of the metastable liquid (homogeneous nucleation). Both processes are affected by contact angle [20]. Carey showed that for surfaces that are oleophilic, the homogeneous nucleation temperature is high and generally over >100 °C [20]. The onset of liquid to gas phase change in Table 3 for the oleophilic particles is 105 °C such that this value is a lower limit estimate for the nucleation temperature because it corresponds to the onset of phase change. Although nucleation temperature is not definitive evidence of homogeneous nucleation, a nucleation temperature of 105 °C does not exclude homogeneous nucleation as a possible mechanism of bubble formation on the oleophilic surfaces. The nucleation temperature observed for the oleophobic particles is much lower, from Table 3, 85 °C. The large difference between nucleation temperatures for the more oleophobic and oleophilic particles suggests that heterogeneous nucleation is occurring on the oleophobic surfaces. Heterogeneous nucleation processes generally promote a greater number of nucleation sites (as opposed to homogeneous nucleation that corresponds to vapor film development on surfaces) [21]. Most models for nucleate pool boiling describe the heat flux (q'') as a power law of the superheat temperature ΔT and the density of active nucleation sites n [21]: $q'' = \Delta T^A\ n^B$ with $1 \le A \le 1.8$ and $0.3 \le B \le 0.5$. Estimating ΔT as 135 – 105 = 30 °C for oleophilic particles and 135 – 85 = 50 °C for oleophobic particles and equivalent nucleation sites for both particles (a conservative estimate), as well as constant values of A and B for the two particles, then the heat flux associated with the oleophobic particles is about 1.5 times greater than for the oleophilic particles.

5. Conclusions

Kerosene droplets with nanoparticle additives of aluminum (Al) functionalized with perfluorohexadecanoic acid (PFHD) self-assembled monolayer were shown to produce higher burn rate constants compared to pure kerosene and compared to kerosene with Al nanoparticles of the same size and concentration. The Al-PFHD particles are oleophobic and were shown to disperse and remain suspended in kerosene for a longer time than Al particles which are oleophilic in kerosene. Measured thermal diffusivity of the mixtures varied negligibly with added particulates indicating the PFHD does not alter thermal transport properties of the mixtures. The oleophobic Al-PFHD particles provide greater phase change heat transfer by increasing the fraction of liquid–vapor contact at the solid–liquid interface. Estimates indicate that oleophobic particles increase phase change heat transfer by 1.5 times. This mechanism reduces the onset of boiling by 50 °C and results in 121% higher burn rate constants in early stage combustion for Al-PFHD in kerosene compared with pure kerosene droplets. The Al particles without coating reduce the onset of boiling by 30 °C and also increase the burn rate constant over pure kerosene by 44% in early stage combustion. The particles replace the heat up stage associated with kerosene and directly promote combustion in early stage. These results show that altering surface particle properties to promote phase change heat transfer reduces evaporation onset temperature and promotes combustion of kerosene.

Acknowledgments

The authors are grateful for support from ARO (and Dr. Ralph Anthenien) under award W911NF-14-1-0250. We are thankful to Mr. Colt Cagle for assistance with LFA measurements and Ms. Richa Padhye for assistance with FTIR measurements.

References

[1] G.P. Sutton, O. Biblarz, Rocket propulsion elements, 8th ed., John Wiley and Sons, 2010.
[2] I. Javed, S.W. Baek, K. Waheed, Effects of dense concentrations of aluminum nanoparticles on the evaporation behavior of kerosene droplet at elevated temperatures: the phenomenon of microexplosion, Exp. Therm. Fluid Sci. 56 (2014) 33–44.
[3] I. Javed, S.W. Baek, K. Waheed, G. Ali, S.O. Cho, Evaporation characteristics of kerosene droplets with dilute concentrations of ligand-protected aluminum nanoparticles at elevated temperatures, Combust. Flame 160 (12) (2013) 2955–2963.
[4] Y. Gan, L. Qiao, Combustion characteristics of fuel droplets with addition of nano and micron-sized aluminum particles, Combust. Flame 158 (2) (2011) 354–368.
[5] B. Van Devener, S.L. Anderson, Breakdown and combustion of JP-10 fuel catalyzed by nanoparticulate CeO2 and Fe2O3, Energy Fuels 20 (5) (2006) 1886–1894.
[6] D. Attinger, C. Frankiewicz, A.R. Betz, T.M. Schutzius, R. Ganguly, A. Das, C.-J. Kim, C.M. Megaridis, Surface engineering for phase change heat transfer: a review, MRS Energy Sustainability 1 (2014) E4.
[7] W.A. Zisman, Relation of the equilibrium contact angle to liquid and solid constitution, Contact angle, wettability, and adhesion, 43 (1964), pp. 1–51.
[8] P. Dagaut, M. Cathonnet, The ignition, oxidation, and combustion of kerosene: a review of experimental and kinetic modeling, Prog. Energy Combust. Sci. 32 (1) (2006) 48–92.
[9] K.S. Kappagantula, C. Farley, M.L. Pantoya, J. Horn, Tuning energetic material reactivity using surface functionalization of aluminum fuels, J. Phys. Chem. C 116 (46) (2012) 24469–24475.
[10] R.J. Jouet, A.D. Warren, D.M. Rosenberg, V.J. Bellitto, K. Park, M.R. Zachariah, Surface passivation of bare aluminum nanoparticles using perfluoroalkyl carboxylic acids, Chem. Mater. 17 (11) (2005) 2987–2996.
[11] J.M. Horn, J.M. Lightstone, J.R. Carney, R.J. Jouet, Preparation and characterization of functionalized aluminum nanoparticles, AIP Conf. Proc. 1426 (2012) (2012) 607–610.
[12] S. Datta, B. Dikici, M.L. Pantoya, S. Ekwaro-Osire, Reaction dynamics and probability study of aluminum-viton-acetone droplets, J. Propul. Power 27 (2) (2011) 396–401.
[13] M.N. Bello, M.L. Pantoya, K. Kappagantula, W.S. Wang, S.A. Vanapalli, D.J. Irvin, L.M. Wood, Reaction Dynamics of rocket propellant with magnesium oxide nanoparticles, Energy Fuels 29 (9) (2015) 6111–6117.
[14] W.M. Haynes, CRC handbook of chemistry and physics, CRC Press, Boca Raton, FL, 2014.
[15] R. Redón, A. Vázquez-Olmos, M.E. Mata-Zamora, A. Ordóñez-Medrano, F. Rivera-Torres, J.M. Saniger, Contact angle studies on anodic porous alumina, Rev. Adv. Mater. Sci. 11 (1) (2006) 79–87.
[16] Y.F. Miura, M. Takenaga, T. Koini, M. Graupe, N. Garg, R.L.J. Graham, T.R. Lee, Wettabilities of self-assembled monolayers generated from CF3-terminated alkanethiols on gold, Langmuir 14 (20) (1998) 5821.
[17] R. Colorado, T.R. Lee, Wettabilities of self-assembled monolayers on gold generated from progressively fluorinated alkanethiols, Langmuir 19 (8) (2003) 3288–3296.
[18] S.R. Turns, An introduction to combustion: concepts and applications, 2nd ed., McGraw-Hill, 2000.
[19] A. Aesar, Research chemicals, metals and materials, A Johnson Matthey Company (2012), pp. 2–5.
[20] V.P. Carey, Liquid-vapor phase-change phenomena, Hemisphere Pub. Corp., Washington, DC, 1992.
[21] V.P. Carey, Liquid-vapor phase-change phenomena, 2nd ed., Taylor and Francis Group, New York, NY, 2008.